

See discussions, stats, and author profiles for this publication at: <https://www.researchgate.net/publication/51194810>

# Fabrication and Characterization of an All-Diamond Tubular Flow Microelectrode for Electroanalysis

ARTICLE in ANALYTICAL CHEMISTRY · JUNE 2011

Impact Factor: 5.64 · DOI: 10.1021/ac2010247 · Source: PubMed

---

CITATIONS

6

READS

44

## 7 AUTHORS, INCLUDING:



Laura A Hutton

Element Six

11 PUBLICATIONS 239 CITATIONS

[SEE PROFILE](#)



Marcio Vidotti

Universidade Federal do Paraná

41 PUBLICATIONS 638 CITATIONS

[SEE PROFILE](#)



Mark Edward Newton

The University of Warwick

105 PUBLICATIONS 1,784 CITATIONS

[SEE PROFILE](#)



Julie V Macpherson

The University of Warwick

175 PUBLICATIONS 5,629 CITATIONS

[SEE PROFILE](#)

# Fabrication and Characterization of an All-Diamond Tubular Flow Microelectrode for Electroanalysis

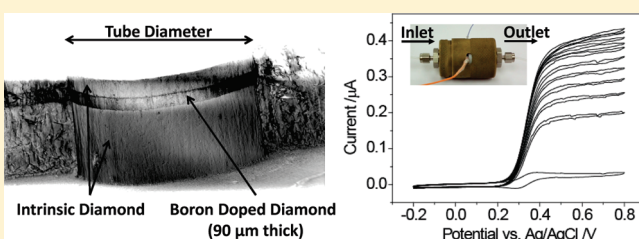
Laura A. Hutton,<sup>†</sup> Marcio Vidotti,<sup>§</sup> James G. Iacobini,<sup>†</sup> Chris Kelly,<sup>||</sup> Mark E. Newton,<sup>\*,‡</sup> Patrick R. Unwin,<sup>†</sup> and Julie V. Macpherson<sup>\*,†</sup>

<sup>†</sup>Department of Chemistry and <sup>‡</sup>Department of Physics, University of Warwick, CV4 7AL, Coventry, U.K.

<sup>§</sup>Departamento de Química, Universidade Federal do Paraná, CP 19081, CEP 81531-980 Curitiba, PR, Brazil

<sup>||</sup>Element Six Ltd., Kings Ride Park, Ascot, Berkshire, SL5 8BP, U.K.

**ABSTRACT:** The development of the first all-diamond hydrodynamic flow device for electroanalytical applications is described. Here alternate layers of intrinsic (insulating), conducting (heavily boron doped), and intrinsic polycrystalline diamond are grown to create a sandwich structure. By laser cutting a hole through the material, it is possible to produce a tubular flow ring electrode of a characteristic length defined by the thickness of the conducting layer (for these studies  $\sim 90 \mu\text{m}$ ). The inside of the tube can be polished to  $17 \pm 10 \text{ nm}$  surface roughness using a diamond impregnated wire resulting in a coplanar, smooth, all-diamond surface. The steady-state limiting current versus volume flow rate characteristics for the one electron oxidation of  $\text{FcTMA}^+$  are in agreement with those expected for laminar flow in a tubular electrode geometry. For dopamine detection, it is shown that the combination of the reduced fouling properties of boron doped diamond, coupled with the flow geometry design where the products of electrolysis are washed away downstream of the electrode, completely eradicates fouling during electrolysis. This paves the way for incorporation of this flow design into online electroanalytical detection systems. Finally, the all diamond tubular flow electrode system described here provides a platform for future developments including the development of ultrathin ring electrodes, multiple apertures for increased current response, and multiple, individually addressable ring electrodes incorporated into the same flow tube.



Poly-crystalline boron doped diamond (pBDD) attracts much interest as an electrode material for electroanalysis,<sup>1,2</sup> due to its very wide potential window in aqueous electrolytes,<sup>3–5</sup> low background currents,<sup>6,7</sup> and resistance to fouling.<sup>8–10</sup> As such, pBDD has been used to detect a wide range of electrochemically active species, from metal ions and inorganics such as lead<sup>11</sup> and sulfides,<sup>12</sup> to organics, including chlorophenols,<sup>13,14</sup> glucose,<sup>15</sup> polyamides,<sup>16</sup> and serotonin.<sup>10</sup> pBDD is also resistant to corrosion under both acidic and alkaline conditions, as well as at extreme positive and negative applied potentials,<sup>17,18</sup> and is stable at high temperatures and pressures.<sup>1</sup>

Typically, macrosized pBDD electrodes ( $\geq 1 \text{ mm}$ ) have been employed for electroanalytical measurements in quiescent solutions<sup>19,20</sup> but to improve sensitivity there has been a push toward miniaturization through the development and application of pBDD-based microelectrodes<sup>4,21–24</sup> and microarrays.<sup>25–28</sup> Alternatively, hydrodynamic techniques can be used to enhance the voltammetric signal. To-date, there have been relatively few hydrodynamic studies employing pBDD electrodes. These include, the analysis of dopamine<sup>29</sup> and nicotinamide adenine dinucleotide<sup>30</sup> using pBDD rotating disk electrodes and the detection of chlorophenol,<sup>31</sup> with BDD channel flow electrodes.<sup>32</sup> pBDD disk microelectrodes have also been used as detectors in capillary electrophoresis and flow injection analysis.<sup>33–35</sup>

A major challenge in the use of pBDD as an electrode material for hydrodynamic (flow) studies is how to encapsulate the

electrode in an insulating support structure to produce a coplanar structure.<sup>24,26,36,37</sup> Recession or protrusion of the electrode surface from the surrounding insulator can significantly affect the flow hydrodynamics and complicate the mass transport characteristics.<sup>38</sup> It is also desirable that the encapsulating insulating material does not limit the wide range of applications, e.g., chemical stability in aggressive environments and at elevated temperatures and pressure, etc. facilitated by the use of BDD as an electrode.

An elegant solution to the challenges outlined is to fabricate all-diamond electrode devices, where the pBDD is insulated with intrinsic diamond. Work in this area to-date has been limited, most likely due to the more complex diamond synthesis and processing procedures required. Nonetheless, the concept has been demonstrated with the development of arrays of all-diamond pBDD disk microelectrodes (MEs). Here a layer of pBDD was grown and patterned to reveal cylindrical-type structures. Subsequent overgrowth with intrinsic diamond and polishing to reveal the tops of the cylinders resulted in all diamond coplanar BDD disk MEs,  $10–50 \mu\text{m}$  in diameter.<sup>39,40</sup>

In this Technical Note we present the first example of a hydrodynamic all-diamond electrode, the tubular flow ME (TFME), for electroanalytical applications. The electrode is

Received: April 21, 2011

Accepted: June 6, 2011

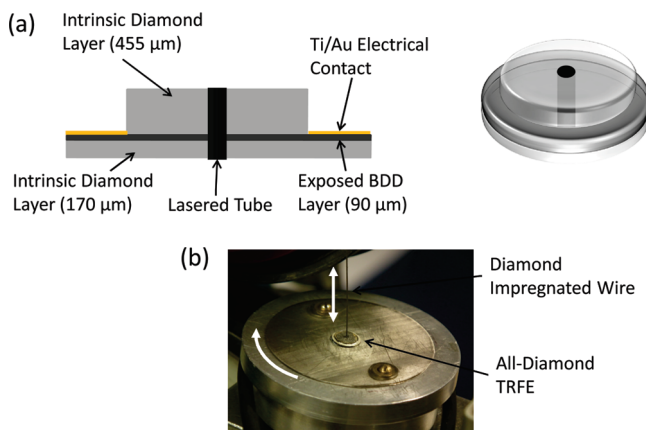


**Figure 1.** (a) Schematic of all-diamond TFME where the BDD layer is sandwiched between two intrinsic diamond layers with a hole lasered vertically through the middle for tubular flow. (b) Photo of the all-diamond TFME polishing setup with the diamond impregnated wire.

fabricated using a three-layered diamond structure comprising a conducting pBDD layer sandwiched between two insulating layers. Laser machining (to define a hole) and further polishing to smooth the inside of the cut surface results in the formation of an all-diamond TFME. The electrodes were characterized and found to give well-defined mass transport over a wide range of flow rates, consistent with a coplanar geometry. This was further verified by microscopy analysis. The electrodes were used for the detection of dopamine and, in contrast to the majority of all other electrodes, showed no signs of passivation due to electrode fouling. Once fabricated, the same TFME could be used repeatedly and reliably with no deterioration in electrode performance.

## ■ EXPERIMENTAL SECTION

The layered polycrystalline diamond samples were prepared by Element Six Ltd. (E6 Ltd., Ascot, U.K.) using a commercial microwave plasma CVD process. The diamond wafer consisted of a  $\sim 455\text{ }\mu\text{m}$  thick layer of mechanical grade chemical vapor deposited (CVD) intrinsic diamond, which was lapped on both sides. Mechanical grade CVD diamond is optically opaque and electrically insulating. A  $\sim 90\text{ }\mu\text{m}$  thick layer of pBDD was grown onto the nucleation face (boron dopant density  $\sim 3 \times 10^{20}\text{ B atoms cm}^{-3}$ , as estimated from electrical resistivity measurements) and then a  $\sim 170\text{ }\mu\text{m}$  layer of intrinsic mechanical grade diamond to fully insulate the boron doped layer. A 355 nm laser micromachining system (E-355H-3-ATHI-O system, Oxford Lasers) was used to cut a 10 mm diameter disk from the diamond wafer and then a hole, 500 μm in diameter, in the center to create the tube (duct) through which solution flows. To enable electrical connection to the conducting pBDD layer, a “top hat” structure (top diameter 6 mm, bottom diameter 10 mm) was created by laser milling through the diamond to expose the pBDD layer, as shown schematically in Figure 1a.

In order to achieve a smooth inner surface and to remove any amorphous carbon deposited during laser cutting, a precision vertical diamond wire saw (Well Diamond Wire Saws Inc.) with a modified sample stage was used to polish the inside of the tube. A 280 μm diameter diamond impregnated wire (MTI Corporation) on a tensional pulley was pulled up and down through the lasered hole, slightly offset so the wire was forced against the inner wall. At the same time, the diamond was rotated on a stage at 60 rpm

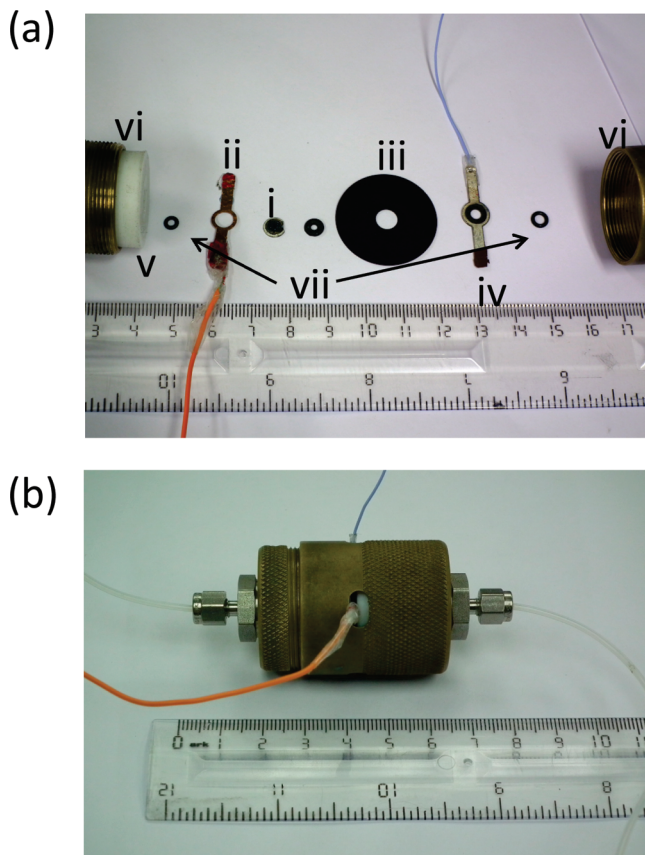


**Figure 2.** Photographs of an all-diamond TFME flow setup; (a) showing the individual components and (b) the completed device, ready to use.

so that an even polish was obtained on all parts of the inner wall of the tube. Figure 1b shows a photograph of the wire passing through the all-diamond TFME.

The TFME was acid-cleaned, as described previously,<sup>41</sup> giving an oxygen-terminated surface. Layers of Ti (10 nm) and Au (400 nm) were sputtered (Moorfield Minibox) onto the outer exposed planar pBDD surface (Figure 1a) and annealed at 475 °C for 4 h. The disassembled and assembled device is shown in parts a and b of Figure 2, respectively. The diamond (labeled i, in Figure 2a) was placed in the flow device setup, and a copper ring connector (Cu foil, 300 μm thick, Goodfellow) with arms on either side (labeled ii) was used to make contact with the (Ti/Au) layer, to provide the external electrical contact to the TFME. A thin polyimide spacer (200 μm thick, Goodfellow, labeled iii) was employed to separate the diamond from a circular Ag/AgCl reference electrode (labeled iv). The copper connector, the polyimide spacer, and the Ag/AgCl electrode were all cut to shape using the laser micromachining system and cleaned, before use, in 0.1 M HCl. The Ag/AgCl electrode was produced by chloridizing Ag foil (500 μm thick, Goodfellow). The electrodes were compressed between two PTFE blocks (labeled v) and held in place with brass housing (labeled vi) which was screwed together (Figure 2b). Stainless steel swagelok tubing fittings (tube o.d. 1/6 in.) with an O-ring seal were mounted into the PTFE blocks to make the inlet and outlet connectors. The device was made water tight with rubber o-rings (labeled vii).

The all-diamond TFME was characterized using field-emission scanning electron microscopy (FE-SEM) using an In-Lens detector at 2 kV (Zeiss Supra55VP), as well as room temperature

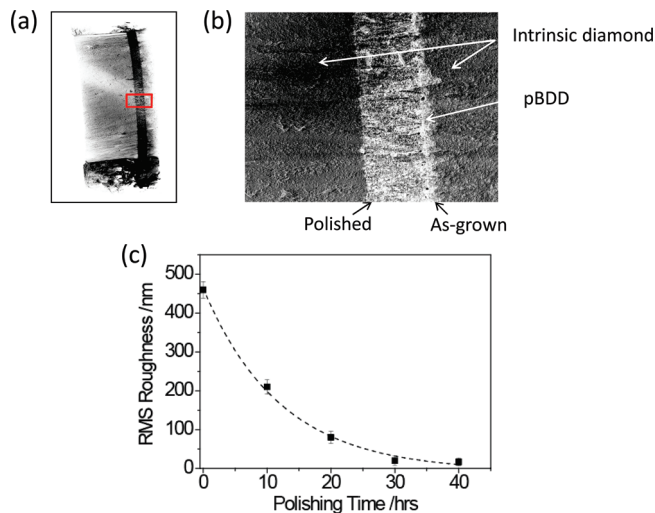


**Figure 3.** FE-SEM images of an all-diamond TFME at (a) low (note contrast inversion) and (b) high resolution. (c) Plot of rms surface roughness, obtained using WLI, as a function of polishing time. The thickness of the pBDD band is  $\sim 90 \mu\text{m}$

micro-Raman spectroscopy (Renishaw inVia Raman Microscope, Renishaw) and white light interferometry (WLI, WYKO NT-2000 surface profiler, WYKO Systems). To test the electrochemical characteristics of the TFME, a solution comprising 0.1 mM ferrocenylmethyl trimethylammonium hexafluorophosphate ( $\text{FcTMA}^+$ ), synthesized in-house, was employed in 0.1 M KCl supporting electrolyte. Further voltammetric experiments were performed using 0.1 mM dopamine hydrochloride (Sigma Aldrich) in 0.1 M phosphate buffer solution (PBS). All solutions were prepared from Milli-Q water (Millipore Corp.), resistivity  $18.2 \text{ M}\Omega \text{ cm}$  at  $25^\circ\text{C}$ . Cyclic voltammetry (CV) was performed in a two-electrode configuration using a CHI750C potentiostat, at  $50 \text{ mV s}^{-1}$ .

## RESULTS AND DISCUSSION

The structure and surface finish of the all-diamond TFMEs were characterized using FE-SEM, WLI, and micro-Raman. This was achieved by cross sectioning the TFME, through the center, using the laser cutter. Figure 3a,b shows low- and high-resolution FE-SEM images of the inside of the TFME. At low resolution, the inner curved structure of the entire TFME is visible. The conducting BDD region is clearly seen as a dark band, sandwiched between the lighter insulating intrinsic diamond. Note that the contrast on the FE-SEM image has been reversed to aid identification.<sup>42</sup> At higher resolution more detailed structure on the intrinsic-doped diamond interface is revealed (no inversion of contrast). The interface between the nucleation face of the BDD layer and the intrinsic diamond is sharp; a consequence of growing the BDD on a lapped diamond surface. In contrast, the interface between the growth face of BDD and the intrinsic diamond is less sharp, as the pBDD face was not lapped before regrowth of the intrinsic layer. This polishing step did not occur to avoid any possible damage to the layered structure, resulting from, e.g., cracking of the disk. However, at both interfaces, growth between the intrinsic/BDD and BDD/intrinsic surfaces appears continuous, which is essential to guarantee a good seal for subsequent voltammetry.

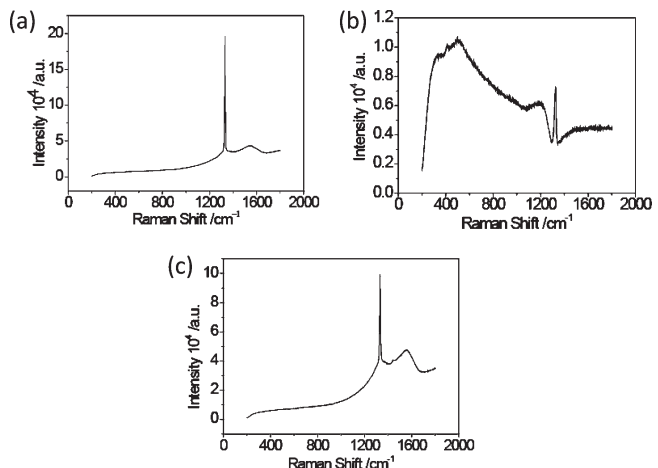


**Figure 4.** Typical Raman spectra for the TFME taken at room temperature with a 514.5 nm laser in the vicinity of (a) entry layer of mechanical grade intrinsic diamond; (b) BDD electrode layer; and (c) the exit layer of mechanical grade intrinsic diamond.

The surface roughness inside the hole was investigated using WLI on five electrodes, which were each subject to a different polishing time. After polishing, the electrode was cut in half in order to determine surface roughness. Figure 3c shows a plot of polishing time versus root-mean-square (rms) surface roughness. Prior to polishing, the inner surface of the laser cut hole revealed a rms surface roughness of  $460 \pm 21 \text{ nm}$ . After 10 h, the surface roughness decreased significantly to a value of  $210 \pm 18 \text{ nm rms}$ . Continued polishing showed a decrease in the surface roughness to  $20 \pm 12 \text{ nm rms}$  (30 h of polishing). After 30 h the rate of polishing seemed to significantly decrease so that after a further 10 h (40 h in total) the surface finish inside the tube had not improved ( $17 \pm 10 \text{ nm}$ ). All further experiments were thus performed using TFMEs which had been polished for  $\geq 30 \text{ h}$ . It is also interesting to note that there are no major features on the WLI cross sections that would indicate that the different layers of diamond (intrinsic and conducting) polish at significantly different rates.

Raman spectra were recorded to analyze the quality and boron content of the polished all-diamond TFME. In the intrinsic diamond regions, either side of the BDD layer, Figure 4a,c, a large diamond ( $\text{sp}^3$ ) peak at  $1332 \text{ cm}^{-1}$  as well as a small broad nondiamond carbon ( $\text{sp}^2$ ) signal at  $1560 \text{ cm}^{-1}$  are seen. The latter is not unexpected given that opaque mechanical grade intrinsic diamond contains defects and intergranular nondiamond carbon.<sup>43</sup> In the region of the boron-doped layer, Figure 4b again shows a diamond ( $\text{sp}^3$ ) peak centered at  $1332 \text{ cm}^{-1}$ , but the asymmetry of the peak (fano resonance) indicates a high boron content ( $\geq 3 \times 10^{20} \text{ atoms cm}^{-3}$ ), in agreement with the electrical resistivity measurements, thus indicating the electrode should exhibit metallic-like conductivity.<sup>44</sup> The conducting BDD layer is evidently of high quality with negligible amounts of  $\text{sp}^2$  carbon impurities. Importantly, the Raman spectrum also indicates any amorphous carbon left from the laser cutting process has been removed after  $\geq 30 \text{ h}$  polishing.

To assess the hydrodynamics of the TFME, CVs were recorded for 0.1 mM  $\text{FcTMA}^+$  in 0.1 M KCl at a scan rate of  $50 \text{ mV s}^{-1}$  under stationary conditions (lowest current) and at various volume flow rates,  $V_\beta$  in the range  $0.028$ – $0.167$  (highest current)  $\text{cm}^3 \text{s}^{-1}$  as shown in Figure 5a. The TFME was orientated such that

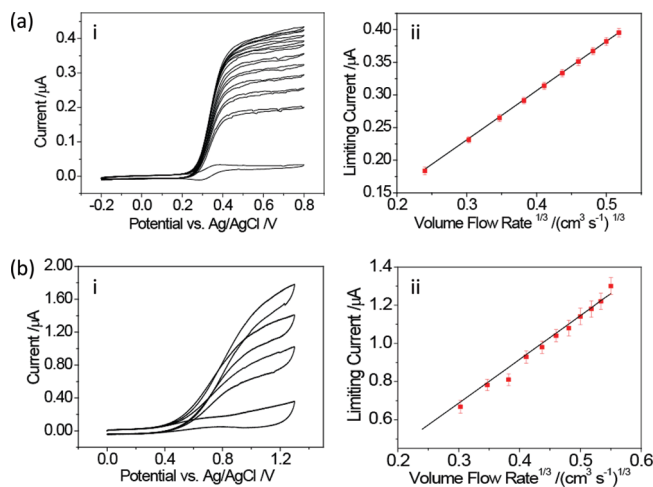


**Figure 5.** (ai) CVs for the oxidation of 0.1 mM  $\text{FcTMA}^+$  in 0.1 M KCl with  $V_f$  of 0 (lowest current), 0.028, 0.056, 0.069, 0.083, 0.097, 0.111, 0.125, 0.139, 0.153, and 0.167 (highest current)  $\text{cm}^3 \text{s}^{-1}$  at a scan rate of  $50 \text{ mV s}^{-1}$ . (a ii) Plot of experimental (red ■) and theoretical (—) steady state current against  $V_f^{1/3}$  for 0.1 mM  $\text{FcTMA}^+$  in 0.1 M KCl. Error bars show the standard deviation of five experiments. (bi) CVs for the oxidation of 0.15 mM dopamine in 0.1 M PBS with  $V_f$  of 0 (lowest current), 0.028, 0.083, and 0.167 (highest current)  $\text{cm}^3 \text{s}^{-1}$  and a scan rate of  $50 \text{ mV s}^{-1}$ . (b ii) Plot of experimental (red ■) and theoretical (—) pseudo steady-state current against  $V_f^{1/3}$  for 0.15 mM dopamine in 0.1 M PBS. Error bars show the standard deviation of five experiments.

solution flow encountered the  $455 \mu\text{m}$  thick layer of intrinsic diamond first. Laminar tubular flow was treated first by Levich<sup>45</sup> and then later by Blaedel and Klatt,<sup>46</sup> who determined that the limiting current response,  $i_{\text{lim}}$  as a function of  $V_f$  for well-developed laminar flow in the axial direction is

$$i_{\text{lim}} = 5.43nFC_bD^{2/3}X^{2/3}V_f^{1/3} \quad (1)$$

where  $n$  is the number of electrons transferred per redox process,  $F$  is the Faraday constant,  $C_b$  is the bulk electroactive species concentration,  $D$  is the diffusion coefficient, and  $X$  is the length of the tubular electrode ( $= 90 \pm 5 \mu\text{m}$ ).

In Figure 5a, a steady-state sigmoidal current response is observed which increases with increasing  $V_f$ . A plot of  $i_{\text{lim}}$  versus  $V_f^{1/3}$  (red ■) gives a straight line response which agrees very well with theory (—), as shown in Figure 5aii, for  $D$  of  $\text{FcTMA}^+ = 6 \times 10^{-6} \text{ cm}^2 \text{s}^{-1}$  and  $n = 1$ . This demonstrates that (i) the entrance length of the TFME is sufficient for laminar Poiseulle flow to be established, and (ii) the pBDD electrode is not significantly recessed or protruding from the insulating diamond surface to affect the laminar flow profile, consistent with the data shown in Figure 3.

The mass transport coefficient,  $k_t$ , can be calculated from

$$k_t = \frac{0.865D^{2/3}V_f^{1/3}}{X^{1/3}R} \quad (2)$$

where  $R$  is the radius of the tube. For the highest  $V_f$  employed here ( $= 0.167 \text{ cm}^3 \text{s}^{-1}$ ),  $R = 250 \mu\text{m}$  and  $k_t = 0.030 \text{ cm s}^{-1}$ , which is a reasonable value for kinetic studies. However, to access fast electron transfer rate constant coefficients, there is considerably scope for achieving higher  $k_t$  values by using ultrathin conducting layers of pBDD coupled with smaller tube diameters in the layered structure. Work in this area is currently in progress.

After initial characterization studies, the TFME was employed to detect the neurotransmitter dopamine. Dopamine oxidation is well-known to result in fouling of the electrode surface resulting in a significant decrease in the expected electrochemical signal, especially after repeated use of the electrode.<sup>47–49</sup> Although, pBDD has been shown to reduce fouling, it does not eradicate the problem in quiescent solution. Figure 5bi shows typical CVs recorded at the all-diamond TFME for the oxidation of 0.15 mM dopamine in 0.1 M PBS at 0 (lowest current), 0.028, 0.083, and 0.167 (highest current)  $\text{cm}^3 \text{s}^{-1}$  flow rates. The electrode was not cleaned in between measurements. As shown in Figure 5bii, the CVs approach a pseudo steady-state plateau. Figure 5bii shows a plot of  $i_{\text{lim}}$  versus  $V_f^{1/3}$  and the corresponding fit to theory (—) assuming  $n = 2$  and  $D = 6 \times 10^{-6} \text{ cm}^2 \text{s}^{-1}$ .<sup>50</sup> Importantly, a linear response is seen, with experimental results agreeing well with theory. Thus, in this flow geometry, where the products of electrolysis can be washed away downstream from the electrode, coupled with the deployment of a pBDD electrode, eradication of electrode fouling, even at this relatively high dopamine concentration used herein, is achieved. Hence, the use of an all-diamond TFME for the online detection of dopamine from *in vivo* analysis<sup>51,52</sup> and digested tissue samples may be realizable. Finally, the same TFME was used continuously for all electrochemical studies, indicating that once fabricated the all-diamond format produces a robust and reproducible electrode arrangement which importantly does not require recalibration between runs.

## CONCLUSIONS

We have described the fabrication and characterization of the first all-diamond hydrodynamic electrode (TFME), comprising a conducting pBDD electrode sandwiched between insulating layers of diamond. With the use of a laser micromachiner to define a hole in the layered material and a diamond impregnated wire to polish the interior of the hole, it is possible to produce an insulating-conducting-insulating tube interior which is coplanar and ultrasMOOTH; WLI reveals a surface roughness of  $\sim 20 \text{ nm}$ .

For a  $500 \mu\text{m}$  diameter tube with a pBDD electrode of length  $\sim 90 \mu\text{m}$  and an intrinsic diamond entrance length of  $\sim 455 \mu\text{m}$ , the steady-state limiting current-volume flow rate characteristics for the oxidation of  $\text{FcTMA}^+$  were found to obey that predicted by Levich for a tubular electrode operating under laminar flow conditions. Application of this flow device to the detection of the neurotransmitter dopamine was shown. Importantly, it has been demonstrated that even at relatively high concentrations of the analyte, the combination of pBDD in this geometry flow system resulted in the eradication of electrode fouling. As this is a common problem with the voltammetric detection of dopamine, this paves the way for use of this flow system in online detection systems.

This platform is extremely promising for significant further work, which will consider (1) significantly increasing mass transport coefficients by employing ultrathin conducting films coupled with smaller diameter holes and (2) developing multiple, individually addressable conducting layer electrodes. The latter will facilitate time-of-flight, generation-collection type experiments aimed at, for example, characterizing the lifetime of transient species, indirect electrochemical determination of the concentration of electroinactive species, etc. (3) Finally by employment of multiple apertures, it will be possible to increase the limiting

current signal for detection of low concentrations of analytes in solution, in a similar manner to UME planar arrays.

## AUTHOR INFORMATION

### Corresponding Author

\*E-mail: j.macpherson@warwick.ac.uk; m.e.newton@warwick.ac.uk

## ACKNOWLEDGMENT

L.A.H. thanks EPSRC/BAE Systems (Mr. David Hankey) for the award of an EPSRC Industrial Case Studentship. J.I. is grateful to the EPSRC/Analytical Fund for Ph.D. funding whilst M.V. thanks the Conselho Nacional de Desenvolvimento Científico e Tecnológico (CNPq), Case Award 200261/2008-8, for financial support. Some of the equipment used in this work was obtained through the Science City Advanced Materials project with support from Advantage West Midlands and the European Regional Development Fund. We would additionally like to thank Element Six Ltd. for providing us with the layered samples, in particular Mr. Jonathan Wilman for growing the layered material. Finally we all thank Mr. Peter Wallis for initial experiments on the layered samples.

## REFERENCES

- (1) Compton, R. G.; Foord, J. S.; Marken, F. *Electroanalysis* **2003**, *15*, 1349.
- (2) Kraft, A. *Int. J. Electrochem. Sci.* **2007**, *2*, 355.
- (3) Panizza, M.; Cerisola, G. *Electrochim. Acta* **2005**, *51*, 191.
- (4) Martin, H. B.; Argoitia, A.; Landau, U.; Anderson, A. B.; Angus, J. C. *J. Electrochem. Soc.* **1996**, *143*, L133.
- (5) Tenne, R.; Levy-Clement, C. *Isr. J. Chem.* **1998**, *38*, 57.
- (6) Pleskov, Y. V.; Mazin, V. M.; Evtseva, Y. E.; Varnin, V. P.; Teremetskaya, I. G.; Laptev, V. A. *Electrochim. Solid State Lett.* **2000**, *3*, 141.
- (7) Yano, T.; Tryk, D. A.; Hashimoto, K.; Fujishima, A. *J. Electrochem. Soc.* **1998**, *145*, 1870.
- (8) Xu, J. S.; Granger, M. C.; Chen, Q. Y.; Strojek, J. W.; Lister, T. E.; Swain, G. M. *Anal. Chem.* **1997**, *69*, A591.
- (9) Sarada, B. V.; Rao, T. N.; Tryk, D. A.; Fujishima, A. *Chem. Lett.* **1999**, *1213*.
- (10) Güell, A. G.; Meadows, K. E.; Unwin, P. R.; Macpherson, J. V. *Phys. Chem. Chem. Phys.* **2010**, *12*, 10108.
- (11) Hutton, L. A.; Newton, M. E.; Unwin, P. R.; Macpherson, J. V. *Anal. Chem.* **2011**, *83*, 735.
- (12) Lawrence, N.; Pagels, M.; Meredith, A.; Jones, T.; Hall, C.; Pickles, C.; Godfried, H.; Banks, C.; Compton, R.; Jiang, L. *Talanta* **2006**, *69*, 829.
- (13) Codognoto, L.; Machado, S. A. S.; Avaca, L. A. *Diamond Relat. Mater.* **2002**, *11*, 1670.
- (14) Zhou, Y.; Zhi, J. *Electrochim. Commun.* **2006**, *8*, 1811.
- (15) Ivandini, T.; Sato, R.; Makide, Y.; Fujishima, A.; Einaga, Y. *Diamond Relat. Mater.* **2004**, *13*, 2003.
- (16) Koppang, M. D.; Witek, M.; Blau, J.; Swain, G. M. *Anal. Chem.* **1999**, *71*, 1188.
- (17) Ramesham, R.; Rose, M. F. *Diamond Relat. Mater.* **1997**, *6*, 17.
- (18) Lee, J.; Tryk, D. A.; Fujishima, A.; Park, S.-M. *Chem. Commun. (Cambridge, U.K.)* **2002**, *486*.
- (19) Granger, M. C.; Witek, M.; Xu, J. S.; Wang, J.; Hupert, M.; Hanks, A.; Koppang, M. D.; Butler, J. E.; Lucaleau, G.; Mermoux, M.; Strojek, J. W.; Swain, G. M. *Anal. Chem.* **2000**, *72*, 3793.
- (20) Spataru, N.; Sarada, B. V.; Popa, E.; Tryk, D. A.; Fujishima, A. *Anal. Chem.* **2001**, *73*, 514.
- (21) Chiku, M.; Watanabe, T.; Einaga, Y. *Diamond Relat. Mater.* **2010**, *19*, 673.
- (22) Sarada, B. V.; Rao, T. N.; Tryk, D. A.; Fujishima, A. *J. Electrochem. Soc.* **1999**, *146*, 1469.
- (23) Cooper, J. B.; Pang, S.; Albin, S.; Zheng, J. L.; Johnson, R. M. *Anal. Chem.* **1998**, *70*, 464.
- (24) Hu, J. P.; Holt, K. B.; Foord, J. S. *Anal. Chem.* **2009**, *81*, 5663.
- (25) Tsunozaki, K.; Einaga, Y.; Rao, T. N.; Fujishima, A. *Chem. Lett.* **2002**, *502*.
- (26) Provent, C.; Haenni, W.; Santoli, E.; Rychen, P. *Electrochim. Acta* **2004**, *49*, 3737.
- (27) Soh, K. L.; Kang, W. P.; Davidson, J. L.; Basu, S.; Wong, Y. M.; Cliffel, D. E.; Bonds, A. B.; Swain, G. M. *Diamond Relat. Mater.* **2004**, *13*, 2009.
- (28) Kang, W. P.; Davidson, J. L.; Wong, Y. M.; Soh, K. L.; Gurbuz, Y. In *Proceedings of the IEEE Sensors 2004*, Vols. 1–3; Rocha, D., Sarro, P. M., Vellekoop, M. J., Eds.; IEEE: New York, 2004; p 376.
- (29) Sopchak, D.; Miller, B.; Kalish, R.; Avyigal, Y.; Shi, X. *Electroanalysis* **2002**, *14*, 473.
- (30) Rao, T. N.; Yagi, I.; Miwa, T.; Tryk, D. A.; Fujishima, A. *Anal. Chem.* **1999**, *71*, 2506.
- (31) Prado, C.; Murcott, G. G.; Marken, F.; Foord, J. S.; Compton, R. G. *Electroanalysis* **2002**, *14*, 975.
- (32) Snowden, M. E.; King, P. H.; Covington, J. A.; Macpherson, J. V.; Unwin, P. R. *Anal. Chem.* **2010**, *82*, 3124.
- (33) Shin, D. C.; Sarada, B. V.; Tryk, D. A.; Fujishima, A. *Anal. Chem.* **2003**, *75*, 530.
- (34) Cvacka, J.; Quaisserova, V.; Park, J.; Show, Y.; Muck, A.; Swain, G. M. *Anal. Chem.* **2003**, *75*, 2678.
- (35) Preechaworapun, A.; Chuanuwatanakul, S.; Einaga, Y.; Grudpan, K.; Motomizu, S.; Chailapakul, O. *Talanta* **2006**, *68*, 1726.
- (36) Holt, K. B.; Hu, J. P.; Foord, J. S. *Anal. Chem.* **2007**, *79*, 2556.
- (37) Soh, K. L.; Kang, W. P.; Davidson, J. L.; Wong, Y. M.; Cliffel, D. E.; Swain, G. M. *Diamond Relat. Mater.* **2008**, *17*, 900.
- (38) Bitziou, E.; Rudd, N. C.; Unwin, P. R. *J. Electroanal. Chem.* **2007**, *602*, 263.
- (39) Pagels, M.; Hall, C. E.; Lawrence, N. S.; Meredith, A.; Jones, T. G. J.; Godfried, H. P.; Pickles, C. S. J.; Wilman, J.; Banks, C. E.; Compton, R. G.; Jiang, L. *Anal. Chem.* **2005**, *77*, 3705.
- (40) Colley, A. L.; Williams, C. G.; Johansson, U. D.; Newton, M. E.; Unwin, P. R.; Wilson, N. R.; Macpherson, J. V. *Anal. Chem.* **2006**, *78*, 2539.
- (41) Hutton, L.; Newton, M. E.; Unwin, P. R.; Macpherson, J. V. *Anal. Chem.* **2009**, *81*, 1023.
- (42) Wilson, N. R.; Clewes, S. L.; Newton, M. E.; Unwin, P. R.; Macpherson, J. V. *J. Phys. Chem. B* **2006**, *110*, 5639.
- (43) Bennett, J. A.; Wang, J.; Show, Y.; Swain, G. M. *J. Electrochim. Soc.* **2004**, *151*, E306.
- (44) Bernard, M. *Diamond Relat. Mater.* **2004**, *13*, 282.
- (45) Levich, V. G. *Physiochemical Hydrodynamics*; Prentice Hall: Englewood Cliffs, NJ, 1962.
- (46) Blaedel, W. J.; Klatt, L. N. *Anal. Chem.* **1966**, *38*, 879.
- (47) Shakthivel, P.; Chen, S.-M. *Biosens. Bioelectron.* **2007**, *22*, 1680.
- (48) Pihel, K.; Walker, Q. D.; Wightman, R. M. *Anal. Chem.* **1996**, *68*, 2084.
- (49) Chuekachang, S.; Kruefu, V.; Chaiyasisit, S.; Phanichphant, S. 5th *IEEE International Conference on Nano/Micro Engineered and Molecular Systems (NEMS)*, 2010; p 133.
- (50) DuVall, S. H.; McCreery, R. L. *J. Am. Chem. Soc.* **2000**, *122*, 6759.
- (51) Murai, S.; Saito, H.; Abe, E.; Nagahama, H.; Miyata, H.; Masuda, Y.; Itoh, T. *Eur. J. Pharmacol.* **1990**, *183*, 417.
- (52) Thomas, D. H.; Taylor, J. D.; Barnaby, O. S.; Hage, D. S. *Clin. Chim. Acta* **2008**, *398*, 63.